Estimating Intracellular Calcium Concentrations and Buffering without Wavelength Ratioing

M. Maravall, Z. F. Mainen, B. L. Sabatini, and K. Svoboda
Cold Spring Harbor Laboratory, Cold Spring Harbor, New York 11724 USA

ABSTRACT We describe a method for determining intracellular free calcium concentration ($[Ca^{2+}]$) from single-wavelength fluorescence signals. In contrast to previous single-wavelength calibration methods, the proposed method does not require independent estimates of resting $[Ca^{2+}]$ but relies on the measurement of fluorescence close to indicator saturation during an experiment. Consequently, it is well suited to $[Ca^{2+}]$ indicators for which saturation can be achieved under physiological conditions. In addition, the method requires that the indicators have large dynamic ranges. Popular indicators such as Calcium Green-1 or Fluo-3 fulfill these conditions. As a test of the method, we measured $[Ca^{2+}]$ in CA1 pyramidal neurons in rat hippocampal slices using Oregon Green BAPTA-1 and 2-photon laser scanning microscopy (BAPTA: 1,2-bis(2-aminophenoxy)ethane-*N*,*N*,*N*′,*N*′-tetraacetic acid). Resting $[Ca^{2+}]$ was 32–59 nM in the proximal apical dendrite. Monitoring action potential-evoked $[Ca^{2+}]$ transients as a function of indicator loading yielded estimates of endogenous buffering capacity (44–80) and peak $[Ca^{2+}]$ changes at zero added buffer (178–312 nM). In young animals (postnatal days 14–17) our results were comparable to previous estimates obtained by ratiometric methods (Helmchen et al., 1996, *Biophys. J.* 70:1069–1081), and no significant differences were seen in older animals (P24–28). We expect our method to be widely applicable to measurements of $[Ca^{2+}]$ and $[Ca^{2+}]$-dependent processes in small neuronal compartments, particularly in the many situations that do not permit wavelength ratio imaging.

INTRODUCTION

The spatial and temporal dynamics of intracellular free calcium ($[Ca^{2+}]$) are crucial to many aspects of neuronal function. Neuronal excitation produces Ca^{2+} influx into the cytoplasm, where Ca^{2+} drives many intracellular signal transduction cascades. In addition, the measurement of $[Ca^{2+}]$ has been used to report on membrane excitation (Regehr et al., 1989; Jaffe et al., 1992; Helmchen et al., 1996; Schiller et al., 1997; Svoboda et al., 1999) and synaptic activation (Muller and Connor, 1991; Murphy et al., 1994; Yuste and Denk, 1995; Denk et al., 1995; Koester and Sakmann, 1998; Mainen et al., 1999b) in small neuronal compartments that are inaccessible to other experimental techniques. Techniques for quantifying $[Ca^{2+}]$ in small structures are therefore of great interest in neurobiology.

The most popular approach to measuring intracellular free $[Ca^{2+}]$ has been ratiometric imaging using the UV-excited $[Ca^{2+}]$ indicator Fura-2 (Grynkiewicz et al., 1985) and its relatives. With this method, $[Ca^{2+}]$ is calculated from a ratio of fluorescences at two excitation wavelengths, $R = F_{\lambda 1}/F_{\lambda 2}$. Taking this ratio facilitates quantitative measurement of $[Ca^{2+}]$ by canceling out optical pathlength, excitation intensity, and detector efficiency. The well-known calibration equation (Grynkiewicz et al., 1985) is

$$\frac{[Ca^{2+}]}{K_D} = \left(\frac{R - R_{min}}{R_{max} - R}\right)\left(\frac{S_{f2}}{S_{b2}}\right) \quad (1)$$

where R_{min} and R_{max} are the ratios at zero and saturating $[Ca^{2+}]$ and S_{f2}/S_{b2} is the ratio of calcium-free over calcium-bound fluorescence intensities at λ_2. The derivation of $[Ca^{2+}]$ thus depends on four parameters that have to be independently calibrated. Using indicators such as Indo-1 (Grynkiewicz et al., 1985), it is also possible to use emission wavelength ratioing.

Several factors conspire to make ratiometric imaging in small structures difficult, especially in intact tissues. Dual-excitation sources are difficult and expensive to implement in laser scanning microscopy, as in two-photon laser scanning microscopy (2PLSM) (Denk et al., 1990; Denk and Svoboda, 1997). The small and noisy fluorescence signals measured from small compartments produce even noisier dual-wavelength ratios, making $[Ca^{2+}]$ estimation prone to considerable errors. In addition, with Fura-2, the need to work with UV excitation light is disadvantageous because it is absorbed by living tissue, producing autofluorescence and photodamage.

Visible-light indicators such as the 1,2-bis(2-aminophenoxy)ethane-*N*,*N*,*N*′,*N*′-tetraacetic acid (BAPTA)-based indicators Oregon Green BAPTA-1 (OGB-1), Calcium Green 1 (Haugland, 1996), Fluo-3 (Minta et al., 1989), and their relatives have thus become increasingly popular. Upon binding to Ca^{2+}, these dyes increase their quantum efficiency without a shift in absorption spectra. The ratios of brightnesses of the calcium bound and unbound forms can be very large (>10), providing the large signal-to-noise ratios required for $[Ca^{2+}]$ imaging in small neuronal structures, such as dendritic spines and axon terminals (Murphy et al., 1994; Yuste and Denk, 1995; Koester and Sakmann, 1998; Mainen et al., 1999b; Schiller et al., 1998). These indicators are well suited to 2PLSM imaging in intact tissue

Received for publication 28 June 1999 and in final form 13 January 2000.
Address reprint requests to Dr. Karel Svoboda, Cold Spring Harbor Laboratory, 1 Bungtown Rd., Cold Spring Harbor, NY 11724. Tel.: 516-367-6878; Fax: 516-367-8866; E-mail: svoboda@cshl.org.

0006-3495/00/05/2655/13 $2.00

(Yuste and Denk, 1995; Koester and Sakmann, 1998; Mainen et al., 1999b) and even in vivo (Svoboda et al., 1997, 1999).

Available visible light indicators do not allow wavelength ratioing (Minta et al., 1989; Tsien and Waggoner, 1995). Instead, signals resulting from $[Ca^{2+}]$ changes ($\Delta[Ca^{2+}]$) are typically expressed as ratios of fluorescence changes over baseline fluorescence, $(f - f_o)/f_o$. As with wavelength ratio measurements, $(f - f_o)/f_o$ is independent of dye concentration, optical path length, excitation intensity, and detector efficiency. However, $(f - f_o)/f_o$ is a sublinear function of $\Delta[Ca^{2+}]$: large changes in $[Ca^{2+}]$ saturate the indicator (Minta et al., 1989; Tsien and Waggoner, 1995; O'Malley et al., 1999). Additionally, $(f - f_o)/f_o$ depends on baseline $[Ca^{2+}]$, $[Ca^{2+}]_0$.

A variety of methods have been devised to translate single-wavelength fluorescence into $[Ca^{2+}]$. For example, $\Delta[Ca^{2+}]$ per action potential was estimated in presynaptic terminals in the cerebellum (Regehr and Atluri, 1995) and the frog tectum (Feller et al., 1996). This calibration is based on the fact that each action potential in a train that saturates the Ca^{2+} indicator contributes the same $\Delta[Ca^{2+}]$. The curve describing the saturation can be used to extract $\Delta[Ca^{2+}]$ per action potential. However, this scheme requires assumptions about resting $[Ca^{2+}]$ or separate ratiometric measurements of this quantity. Similar requirements are shared by other methods (Minta et al., 1989; Jaffe et al., 1992; Lev-Ram et al., 1992; O'Malley, 1994; Schiller et al., 1995; Lau et al., 1999). Kao et al. (1989) introduced a variation on this approach that requires the use of Ca^{2+} ionophores, which is irreversible and impractical in intact tissue. An interesting alternative employed in frog muscle fibers used simultaneous absorption and fluorescence measurements to estimate resting $[Ca^{2+}]$ (Harkins et al., 1993; Kurebayashi et al., 1993). However, absorbance measurements are not practical at the length scale of subneuronal compartments, especially in intact tissue.

We describe an alternative approach that is particularly useful for measurements in small structures and is most easily implemented by using high-affinity indicators with a large dynamic range. It involves the calibration of a smaller number of parameters than previous methods and does not require prior assumptions or calibration of resting $[Ca^{2+}]$. Moreover, it naturally yields estimates of resting $[Ca^{2+}]$ in addition to estimates of $\Delta[Ca^{2+}]$. The key parameter that needs to be determined as part of an experiment is the fluorescence at saturating $[Ca^{2+}]$. The method also relies on estimates of the dynamic range and dissociation constant of the indicator; these are properties of the indicator and need not be repeated for every experiment. We introduce a practical procedure for evaluating these parameters under physiologically reasonable conditions with high-affinity, large dynamic range indicators such as OGB-1. We also discuss how the resulting estimates of $[Ca^{2+}]$ are robust in the face of small errors in parameter calibration (Appendix B). The method provides a practical way to measure absolute resting $[Ca^{2+}]$ and $[Ca^{2+}]$ transient amplitudes in CA1 pyramidal neurons, as well as to compute Ca^{2+} buffering capacity in these neurons.

THEORY: RELATIONSHIP BETWEEN FLUORESCENCE AND $[Ca^{2+}]$

The relationship between single-wavelength fluorescence and $[Ca^{2+}]$ (Tsien, 1989) is straightforward to compute when Ca^{2+} is in equilibrium with an indicator (>2 ms; Sabatini and Regehr, 1998). The relationship between free $[Ca^{2+}]$ and the concentration of Ca^{2+} bound to the fluorophore, [FCa], is given by the law of mass action:

$$[FCa] = \frac{[F]_T[Ca^{2+}]}{K_D + [Ca^{2+}]}. \quad (2)$$

Fluorescence for a single-wavelength dye can be written as $f = S_F[F] + S_{FCa}[FCa] = S_F[F]_T + (S_{FCa} - S_F)[FCa]$, where S_F and S_{FCa} are coefficients describing the brightnesses of the indicator's unbound and bound forms, and $[F]_T$ is its total concentration. Because fluorescence intensities at maximum and minimum $[Ca^{2+}]$ are given by $f_{max} = S_{FCa}[F]_T$ and $f_{min} = S_F[F]_T$, respectively, it follows that $[Ca^{2+}]$ can be expressed as (Tsien, 1989)

$$\frac{[Ca^{2+}]}{K_D} = \frac{f - f_{min}}{f_{max} - f}. \quad (3)$$

This relationship is difficult to use in practice, mainly because f_{min} cannot be evaluated in situ under the same conditions as the measurements of interest, because it requires the reduction of resting $[Ca^{2+}]$ (O'Malley et al., 1999). Furthermore, it is not clear where experimental measurements fall within the range of the indicator: the fluorescence at rest, f_0, can differ from f_{min} in an uncontrolled way. The reason for this is that cellular resting $[Ca^{2+}]$ levels appear to vary widely (20–200 nM) (Nakajima et al., 1993) and depend on the state and type of the cell and the quality of the recording (Kennedy and Thomas, 1996; O'Malley et al., 1999). Such resting levels are far from negligible for high-affinity calcium indicators ($K_D \approx 200$ nM), typically making f_0 much larger than f_{min}.

However, Eq. 3 becomes more illuminating if it is recast in terms of the indicator's dynamic range, $R_f = f_{max}/f_{min}$.

$$\frac{[Ca^{2+}]}{K_D} = \frac{f/f_{max} - 1/R_f}{1 - f/f_{max}}. \quad (4)$$

For indicators with a large dynamic range the exact value of R_f is insignificant, because the term $1/R_f$ will typically be much smaller than f/f_{max}. This situation applies for Fluo-3 ($R_f \approx 50$–200, $K_D \approx 500$ nM; Harkins et al., 1993) and for Fluo 4 ($R_f \approx 85$–100, $K_D \approx 300$ nM, unpublished data) and is schematically illustrated in Fig. 1 *A*. Thus for Fluo-3 and

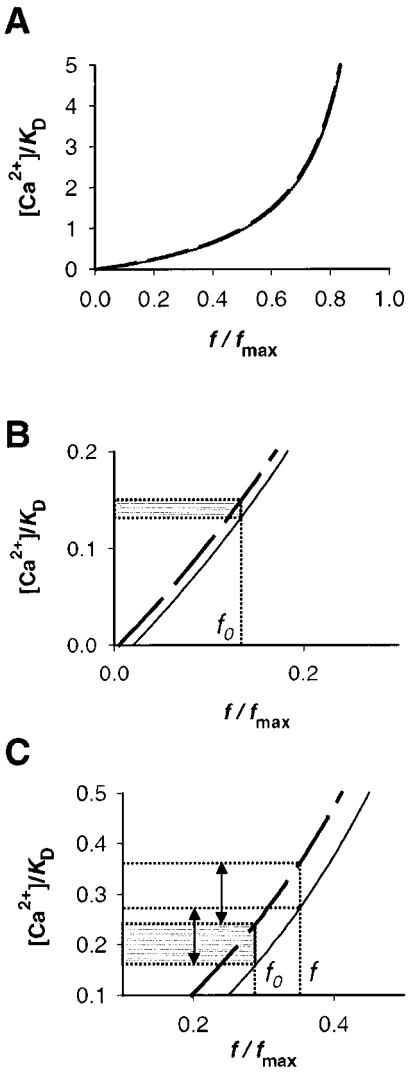

FIGURE 1 Schematic representation of $[Ca^{2+}]$ estimation based on measurements of R_f and f_{max}. (*A*) Relationship between fluorescence (f/f_{max}) and $[Ca^{2+}]$ (units of K_D). The case of very large R_f is illustrated, approximating the properties of Fluo-3. For a good lot of Fluo-3 $R_f \approx$ 100–200 in vitro (Harkins et al., 1993) and perhaps 40% less in cytoplasm (O'Malley et al., 1999). *Solid line*, $R_f = 50$; *long dashed line*, $R_f = 200$. (*B*) Determination of $[Ca^{2+}]_0$ from resting fluorescence f_0 (rescaled from *A*). The gray zone indicates the range of possible values of $[Ca^{2+}]_0$ based on the uncertainty in R_f. Note that $[Ca^{2+}]_0$ can be determined to ~10% precision, even while R_f is subject to a variation of a factor of 4. (*C*) Same determination, for the case of intermediate R_f, illustrated for R_f and K_D approximating the properties of OGB-1: according to our measurements $R_f \approx 8.5$ in cuvette and >5.7 in situ (*solid line*, $R_f = 5.7$; *long dashed line*, $R_f = 8.5$). The gray zone indicates the possible values of $[Ca^{2+}]_0$ based on the uncertainty in R_f. Compared to the uncertainty in absolute $[Ca^{2+}]$ (~40%), the fractional error in the estimation of $\Delta[Ca^{2+}]$ (*arrows*) from $\Delta f \equiv (f - f_0)$ is much smaller, <10%; it is indicated by the difference in the lengths of arrows.

similar indicators an estimate of f_{max} will suffice to measure absolute $[Ca^{2+}]$. For indicators with more modest dynamic ranges, such as OGB-1, R_f does have to be considered and must be estimated in situ (Fig. 1 *B*). However, the dynamic range is a property of the indicator and as such does not depend on resting $[Ca^{2+}]$ and other factors that may vary between cells. Therefore it need not be determined in every experiment. This also holds for the indicator dissociation constant. Also, the dependence of Eq. 4 on the fluorescence f is only through its ratio with f_{max}, eliminating dependences on absolute fluorescence (and hence dye concentration, optical path length, excitation intensity, and detector efficiency).

Changes in $[Ca^{2+}]$, $\Delta[Ca^{2+}] \equiv [Ca^{2+}] - [Ca^{2+}]_0$, associated with changes in fluorescence from baseline, $\delta f \equiv (f - f_0)/f_0$, are given by

$$\frac{\Delta[Ca^{2+}]}{K_D} = \frac{f_{max}}{f_0}(1 - R_f^{-1})\frac{\delta f}{(\delta f_{max} - \delta f)\delta f_{max}}. \quad (5)$$

Compared to Eq. 4, Eq. 5 depends even more weakly on R_f and is thus more robust against uncertainties in this quantity (see Appendix B). This is illustrated in Fig. 1 *C*, where $[Ca^{2+}]$ and $\Delta[Ca^{2+}]$ are "computed" geometrically.

Quantitation of $[Ca^{2+}]$ and of $\Delta[Ca^{2+}]$ based on Eqs. 4 and 5 depends on calibration of the parameters R_f and δf_{max}, and of the dissociation constant K_D (which enters only as a scaling factor). δf_{max} depends on factors that may vary between neurons, in particular resting $[Ca^{2+}]$, $[Ca^{2+}]_0$. Its dependence on $[Ca^{2+}]_0$ is reflected in the equation

$$\delta f_{max} = \frac{(1 - R_f^{-1})}{R_f^{-1} + [Ca^{2+}]_0/K_D}, \quad (6)$$

which follows directly from the relationship between fluorescence and $[Ca^{2+}]$, assuming that true saturation is reached. Inverting the relationship between δf_{max} and $[Ca^{2+}]_0$ provides a useful way to estimate resting $[Ca^{2+}]$:

$$\frac{[Ca^{2+}]_0}{K_D} = \frac{(1 - R_f^{-1})}{\delta f_{max}} - R_f^{-1}. \quad (7)$$

MATERIALS AND METHODS

Brain slice preparation and recording conditions

Hippocampal slices were prepared from juvenile rats (postnatal age (PND) 14–30 days) in accordance with animal care and use guidelines of Cold Spring Harbor Laboratory. The brain was removed, sections of brain containing the hippocampus were blocked, and 300-μm-thick slices were cut on a Vibratome (TPI, St. Louis, MO). These procedures were carried out with the brain submerged in a chilled (2–5°C) cutting solution bubbled with carbogen (95% O_2/5% CO_2). The cutting solution contained (in mM) 110 choline chloride, 25 $NaHCO_3$, 25 D-glucose, 11.6 Na ascorbate, 7 $MgSO_4$, 3.1 Na pyruvate, 2.5 KCl, 1.25 NaH_2PO_4, and 0.5 $CaCl_2$. Slices were then transferred to a submerged holding chamber containing normal artificial cerebrospinal fluid (ACSF), incubated at 35°C for 30–60 min, and then held at room temperature until used. The composition of the normal ACSF was (in mM) 127 NaCl, 25 $NaHCO_3$, 25 D-glucose, 2.5 KCl, 2 $CaCl_2$, 1 $MgSO_4$, and 1.25 NaH_2PO_4. Experiments were performed at 35 ± 1°C. Patch electrodes (3–5 MΩ) were filled with a solution containing (in mM) 135 K methylsulfonate, 10 HEPES, 10 Na phosphocreatine, 4 $MgCl_2$, 4 Na_2ATP, 0.4 NaGTP. Oregon Green BAPTA-1 or Magnesium

Green (MG) (both 100 μM; Molecular Probes, Eugene, OR) were added to the internal solution; occasionally pipettes were tip-loaded with indicator-free solution to prevent dye leakage into the extracellular medium.

Two-photon imaging and electrophysiology

We used a custom-built 2PLSM (Mainen et al., 1999a). A Ti:sapphire laser (Tsunami; Spectra Physics, Mountain View, CA) pumped by a 10-W argon ion laser (Millenia X; Spectra Physics) was tuned to $\lambda \approx 810$ nm and delivered ~100-fs pulses at 80 MHz. The scanning mirrors (model 6800; Cambridge Instruments, Cambridge, MA) were imaged into the backfocal plane of the objective (60×, NA 0.9; Zeiss, Jena, Germany) by a scan lens and the microscope tube lens (both from Zeiss). Fluorescence was detected in epifluorescence and transfluorescence (through an oil-immersion condenser, NA 1.4; Zeiss) modes using photomultiplier tubes (R3896; Hamamatsu, Hamamatsu City, Japan) and combined using a summing amplifier. Laser-scanning differential interference contrast (DIC) was implemented by the addition of a dichroic mirror and a photodiode in the transfluorescence path. Image acquisition was controlled by custom software (Ray Stepnoski, Bell Laboratories, Lucent Technologies).

Whole-cell recordings were obtained under visual guidance, using infrared DIC optics and a CCD camera. Dendrites of CA1 pyramidal neurons were imaged 30–70 μm from the soma. Action potentials were evoked in current clamp mode, using brief (4 ms) current pulses. Electrophysiological data acquisition was performed using an AD-DA board (PCI-MIO-16E-4) and custom software written in LabView (both from National Instruments, Austin, TX) and in Igor (WaveMetrics, Lake Oswego, OR). Fluorescence images were analyzed using custom software written in IDL (Research Systems, Boulder, CO) and Igor. Typically line scan images were collected at 500 Hz.

Fluorescence measurements started ~2 min after break-in and ended when loading approached a steady state ~40 min later. Dye loading was monitored by measuring resting fluorescence, f_0. Steady state was reached when the intracellular dye concentration equilibrated with the pipette concentration. Slice drift caused loss of focus and slight decreases in f_0, which were corrected by refocusing during experiments. These decreasing values of f_0 were ignored when exponential fits to the loading time course were made.

During each measurement trial of action potential-evoked calcium transients, f_0 was determined by averaging fluorescence over at least 128 ms. Peak amplitudes of fluorescence transients were calculated by averaging over 15 ms after the stimulus, or over a 100–120-ms plateau in the case of saturating transients evoked by trains. The background signal was mainly due to photomultiplier tube dark currents and autofluorescence and was subtracted. Fluorescence time series were extracted by averaging across the remaining spatial dimension of the line scan image of the apical dendrite.

Parameter calibration

Estimation of $[Ca^{2+}]$ from fluorescence demands calibration of the parameters R_f, K_D, and δf_{max} (Eqs. 4 and 5). R_f and K_D are properties of the indicator in a particular environment and are not expected to vary across cells. It has been pointed out that R_f may be smaller in cells than in measurement cuvettes, perhaps because of interactions between the indicator and cytoplasmic proteins (Harkins et al., 1993; O'Malley et al., 1999); it should also be noted that the dynamic range may vary from batch to batch for some indicators (Harkins et al., 1993). Similarly, the dissociation constant, K_D, may be affected by the environment (Busa, 1992). It is therefore important to estimate these parameters in a medium that is as close as possible to the cytoplasmic environment.

R_f and K_D were determined in a cuvette fluorometer at 35°C, pH 7.3, using calibration solutions prepared according to standard procedures (Tsien and Pozzan, 1989). $[Ca^{2+}]$ was clamped by EGTA (10 mM) or BAPTA (5 mM) for OGB, and by HEDTA (10 mM) in the case of Magnesium Green (MG). Solutions contained a small amount of indicator (5 μM, or 10 μM for MG) and (in mM) 135 K methylsulfonate, 10 HEPES, and 4 $MgCl_2$, which is identical to the electrode solution. Free $[Ca^{2+}]$ was computed using the MaxChelator program (Bers et al., 1994) (http://www.stanford.edu/~cpatton/maxc.html). Measurements performed with BAPTA and EGTA buffering produced consistent results. In all cases where comparisons have been made, cuvette measurements of R_f have been seen to provide an upper bound on R_f in the cell (Harkins et al., 1993; O'Malley et al., 1999).

Lower bounds on the intracellular R_f were obtained in cultured rat hippocampal slices (P7, 3–5 days in vitro) because in this preparation healthy neurons can be found close to the surface of the slice, allowing more efficient exchange of extracellular solutions. Whole-cell recordings were performed in normal ACSF until dye loading reached steady state, at which point f_{max} was measured. ACSF was then replaced by zero-$[Ca^{2+}]$ ACSF containing 10 mM EGTA, which clamped $[Ca^{2+}]$, causing a decrease in f_0. After reaching steady state, the resting fluorescence corresponding to minimal resting $[Ca^{2+}]$, f_{0min}, was measured, and an estimate of the dynamic range was computed as $R_f \approx f_{max}/f_{0min}$. Because intracellular $[Ca^{2+}]$ could not be fully clamped to zero with this method, this estimate was taken as a lower bound on R_f complementary to the upper bound from cuvette measurements. No attempts were made to estimate K_D in situ.

Intracellular estimates of δf_{max} were made during experiments by transiently flooding neurons with Ca^{2+} by stimulation with rapid trains of action potentials (APs). During AP trains fluorescence transient amplitudes due to successive APs diminished as fluorescence increased. After several APs a saturating fluorescence plateau was reached, suggesting saturation of the Ca^{2+} indicator. To test for indicator saturation, fluorescence transients produced by trains at several different frequencies were compared. In a regime far from indicator saturation, the plateau fluorescence at a given AP frequency would be proportional to that frequency, following $\Delta[Ca^{2+}]$ (Regehr et al., 1994; Helmchen et al., 1996); in contrast, if the indicator was in fact saturated, then plateau fluorescence would be independent of frequency. Typical trains lasted for 360 ms and had frequencies of 56–83 Hz. To check whether the underlying $[Ca^{2+}]$ accumulations increased in proportion to AP frequency, experiments were repeated under identical conditions with the low-affinity indicator MG, which has a dissociation constant almost two orders of magnitude larger than OGB-1 (Haugland, 1996).

Errors quoted denote SEM unless specified otherwise.

Single-compartment model of calcium dynamics

To derive estimates of cellular buffer capacities, we used a simple one-compartment model of cellular $[Ca^{2+}]$ dynamics (Neher and Augustine, 1992; Helmchen et al., 1996). $[Ca^{2+}]$ transients produced by brief, small Ca^{2+} currents, such as those produced by single action potentials (at time $t = t_{AP}$), reach peak values:

$$\Delta[Ca^{2+}] \equiv [Ca^{2+}](t_{AP}) - [Ca^{2+}]_0 = \frac{\Delta[Ca^{2+}]_T}{(1 + \kappa_B + \kappa_F)}. \quad (8)$$

Here $\Delta[Ca^{2+}]_T$ is the total Ca^{2+} influx due to a single action potential, and κ_B and κ_F are the endogenous and added buffer capacities, defined as

$$\kappa_X = \left.\frac{\partial[XCa]}{\partial[Ca^{2+}]}\right|_{rest} = \frac{K_D^{(X)}[X]_T}{(K_D^{(X)} + [Ca^{2+}]_0)^2}. \quad (9)$$

Buffer capacities give the ratio of calcium sequestered by a buffer over calcium that remains free upon a rise in $[Ca^{2+}]$. Here we used the

differential form of these quantities (Neher and Augustine, 1992),

$$\kappa_X = \left.\frac{\Delta[XCa]}{\Delta[Ca^{2+}]}\right|_{transient} = \frac{K_D^{(X)}[X]_T}{(K_D^{(X)} + [Ca^{2+}]_0)(K_D^{(X)} + [Ca^{2+}]_{peak})}. \quad (10)$$

RESULTS

To estimate $[Ca^{2+}]$, equations were formulated expressing $[Ca^{2+}]_0$ and $\Delta[Ca^{2+}]$ in terms of fluorescence and R_f, K_D, and δf_{max} (Eqs. 5 and 6). The determination of these parameters can be constrained sufficiently well to allow accurate measurement of $[Ca^{2+}]$. We tested this method by measuring $[Ca^{2+}]_0$ and the amplitudes of action potential-evoked dendritic $[Ca^{2+}]$ transients in CA1 pyramidal cell dendrites as a function of added buffer capacity.

Parameter calibration

Indicator parameters R_f and K_D were calibrated in vitro under conditions mimicking those of experiments (pipette intracellular solution, 35°C, pH 7.3). R_f was also estimated intracellularly.

The properties of OGB-1 are summarized in Table 1. (Similar cuvette measurements carried out for OGB-2 gave the following values in intracellular solution: $K_D = 295 \pm 13$ nM and $R_f \cong 16 \pm 0.5$, $n = 8$.) Because intracellular measurements ($R_f \approx 4.3$–5.7) necessarily gave a lower bound for R_f, we concluded that the true cytoplasmic value for the dynamic range of the indicator was above the higher of these values, in the range $R_f \approx 5.7$–8.5.

The dissociation constant of MG was 50 times larger than that of OGB-1: $K_D = 10 \pm 2$ μM ($n = 4$).

2PLSM fluorescence imaging in CA1 apical dendrites

CA1 pyramidal cells were loaded with OGB-1 via patch pipette (Fig. 2 *A*). One or two minutes after break-in, the proximal apical dendrite was visible in the 2PLSM image (Fig. 2 *B*). To image fluorescence with good time resolution in the dendrite, we used line scan imaging (Fig. 2 *C*). We then averaged across a window along the spatial axis of the image to arrive at a fluorescence time series (Fig. 2 *D*).

TABLE 1 Properties of the indicator Oregon green BAPTA-1

Parameter	Value	*N*
R_f (cuvette)	8.5 ± 0.7	8
R_f (in situ)	4.3–5.7	3
K_D (cuvette) (nM)	206 ± 5	8

Measurements were performed as described in Materials and Methods. In situ R_f is given as a range: the largest value was adopted as a best estimate because it reflects the best clamping of $[Ca^{2+}]$ to a low level for the estimation of f_{min}.

Single action potentials evoked by somatic current injections caused fluorescence changes due to Ca^{2+} influx through voltage-sensitive calcium channels (Markram et al., 1995). The rise time of single-AP fluorescence changes was <2 ms, while the decay time was in the range of 50–500 ms, depending on indicator concentration (Markram et al., 1995; Helmchen et al., 1996); decay times became longer as Ca^{2+} was increasingly buffered.

Saturating fluorescence transients

To estimate δf_{max}, we relied on the fact that rapid trains of APs produce large $[Ca^{2+}]$ accumulations and that these accumulations increase with AP frequency (Helmchen et al., 1996; Regehr et al., 1994). We confirmed these findings under our experimental conditions, using fluorescence measurements with the low-affinity indicator MG. Because this indicator's K_D is ~50-fold higher than that of OGB-1, it responds linearly to $[Ca^{2+}]$ changes over a much wider range. Indeed, MG fluorescence transient amplitudes increased with AP frequency up to at least 83 Hz (Fig. 3 *A*), approximately in a linear fashion (Fig. 3 *B*). This confirmed that $[Ca^{2+}]$ accumulations continue to grow with AP frequency.

To estimate the maximum OGB-1 fluorescence transient, δf_{max}, during experiments, we measured fluorescence changes produced by the large $[Ca^{2+}]$ accumulations evoked by rapid trains of APs. We attempted to determine whether indicator saturation was in fact reached during these trains by measuring fluorescence levels reached at peak $[Ca^{2+}]$ for several AP frequencies. In contrast to the MG transients, transients obtained with OGB-1 saturated at a steady-state or plateau level, δf_{plt}, over the same range of frequencies (Fig. 3, *A* and *B*), implying that OGB-1 was close to saturation.

However, OGB-1 fluorescence transients due to successive action potentials in a train could still be resolved, even at the highest stimulation frequencies (Fig. 3 *A*; see also Fig. 4 *C*, *inset*). Fluorescence transient peaks following APs were ~4% higher than the corresponding average plateau fluorescence, δf_{plt}, implying that δf_{plt} remained under δf_{max}, even at the highest frequencies probed. To assess the quality of our estimate of δf_{max} we thus performed additional analyses.

One approach made use of the data of Fig. 3, *A* and *B*, which imply that changes in MG fluorescence are proportional to $\Delta[Ca^{2+}]$ over the range of frequencies used in our experiments. We used this relationship to quantify the degree of OGB-1 saturation. As expected, plotting OGB-1 fluorescence amplitudes against MG fluorescence amplitudes gave a hyperbolic relationship, because MG fluorescence is a measure of $\Delta[Ca^{2+}]$. A hyperbolic fit provided an estimate of the degree of saturation corresponding to a particular frequency across cells (Fig. 3 *C*). We define the degree of saturation at frequency ν as $x = 100 \times \delta f_{plt}/\delta f_{max}$,

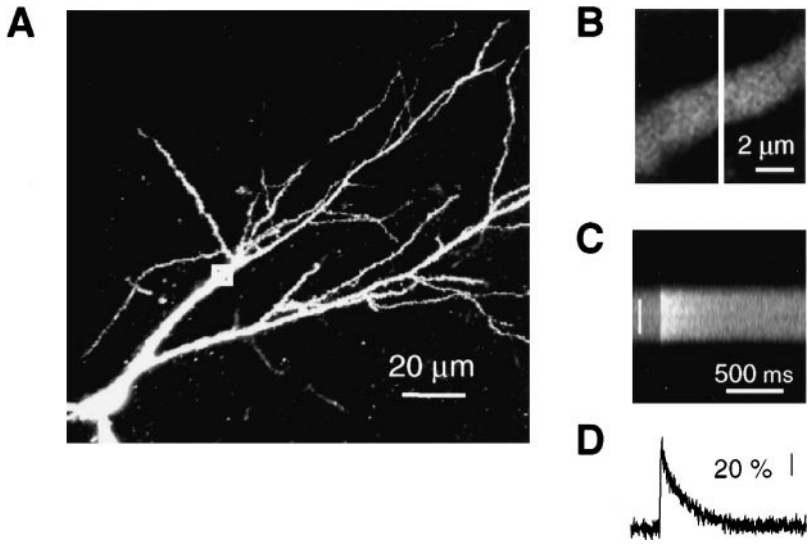

FIGURE 2 2PLSM imaging in brain slices. (*A*) CA1 pyramidal neuron labeled with 100 μM OGB-1 imaged at the end of an experiment. The white square on the apical dendrite indicates the approximate location of the region where measurements were carried out. (*B*) Close-up of proximal apical dendrite from a CA1 neuron; the white line indicates the position of the line scan. (*C*) Line-scan image, showing a transient fluorescence increase due to calcium influx evoked by a single action potential. The white line indicates the size of the averaging window for the fluorescence time series. (*D*) Fluorescence averaged across the dendrite as a function of time.

such that x ranges from 0% (linear regime) to 100% (complete saturation). For the maximum frequency used in these experiments (83 Hz), $x = 89 \pm 3\%$ ($n = 4$). For typical frequencies (67 Hz), $x = 87 \pm 3\%$ ($n = 4$).

A second independent approach allowed us to estimate the degree of saturation reached for each experiment by making use of the proportionality of peak $[Ca^{2+}]$ accumulation to AP frequency (Fig. 3 *B*). This proportionality implies that the ratio of $[Ca^{2+}]$ accumulations produced at AP frequencies ν_2 and ν_1 is ν_2/ν_1. Under conditions close to indicator saturation, the corresponding ratio of fluorescence plateaus, $Q \equiv (\delta f_{plt})_{\nu 2}/(\delta f_{plt})_{\nu 1}$, is not equal to ν_2/ν_1: it is close to but not quite equal to 1 ($Q < \sim 1$). Supposing ν_2 is the higher frequency, its degree of saturation can be expressed (Appendix A) as

$$x = 100 \times \frac{1 - Q\nu_1/\nu_2}{1 - \nu_1/\nu_2}. \qquad (11)$$

With full saturation, the ratio of plateaus at different frequencies would by definition be $Q = 1$, implying $x = 100\%$ also. In contrast, averaging over the highest AP frequencies used in our experiments ($n = 13$ cells), we found $x = 85 \pm 4\%$, in agreement with the previous estimate involving OGB-1 transients versus MG transients (which does not require assuming proportionality to frequency). Using Eq. 11, it was possible to estimate the true maximum fluorescence transient as $\delta f_{max} = \delta f_{plt} \times 100/x$ for each neuron. The results in the remainder of the paper were computed using this correction.

$[Ca^{2+}]$ in CA1 pyramidal neurons

Fluorescence measurements began approximately 2 min after break-in. As found previously (Helmchen et al., 1996), baseline fluorescence intensity then increased with the concentration of intracellular dye until it reached a steady state (Fig. 4 *A*) (with a time constant of 12.5 $\pm$ 2.3 min; $n = 7$).

Transients evoked by single action potentials were measured during dye loading. As predicted by Eq. 8, transient amplitudes decreased with time as the added buffer capacity increased (Fig. 4 *B*), while their durations increased (see also Helmchen et al., 1996). Maximum fluorescence was also measured during dye loading (Table 2). If the action potential trains actually saturated the indicator, the saturating fluorescence ratio, $\delta f_{max} \equiv (f_{max} - f_0)/f_0$, was expected not to vary with loading because it is independent of $[F]_T$ (Eq. 6). For many cells ($n = 15$ out of $n = 28$) we in fact found a constant δf_{max} over 35–50 min (Fig. 4 *C*). In contrast, δf evoked by single APs always decreased with increasing added buffer capacity (Fig. 4 *D*).

However, in some neurons baseline fluorescence did not appear to reach steady state (Fig. 5 *A*), and δf_{max} decreased with time (Fig. 5 *B*). Because of the dependence of δf_{max} on $[Ca^{2+}]_0$ and on R_f, it is likely that this effect was due either to an increase in $[Ca^{2+}]_0$ or to photodamage producing increased baseline fluorescence (and a degradation of R_f) (Koester et al., 1999). We were able to distinguish between these possibilities because changes in $[Ca^{2+}]_0$ are unlikely to be local, while photodamage is spatially highly restricted (Koester et al., 1999), enabling recovery of δf_{max} by moving to adjacent positions on the dendrite (Fig. 5 *C*). The constancy of δf_{max} during an experiment could thus be used as a check on $[Ca^{2+}]_0$ maintenance and cell health.

Resting calcium concentration

Using Eq. 7, we found $[Ca^{2+}]_0$ to be in the range of 37 $\pm$ 5 nM ($R_f \approx 5.7$) to 54 $\pm$ 5 nM ($R_f \approx 8.5$) ($n = 12$).

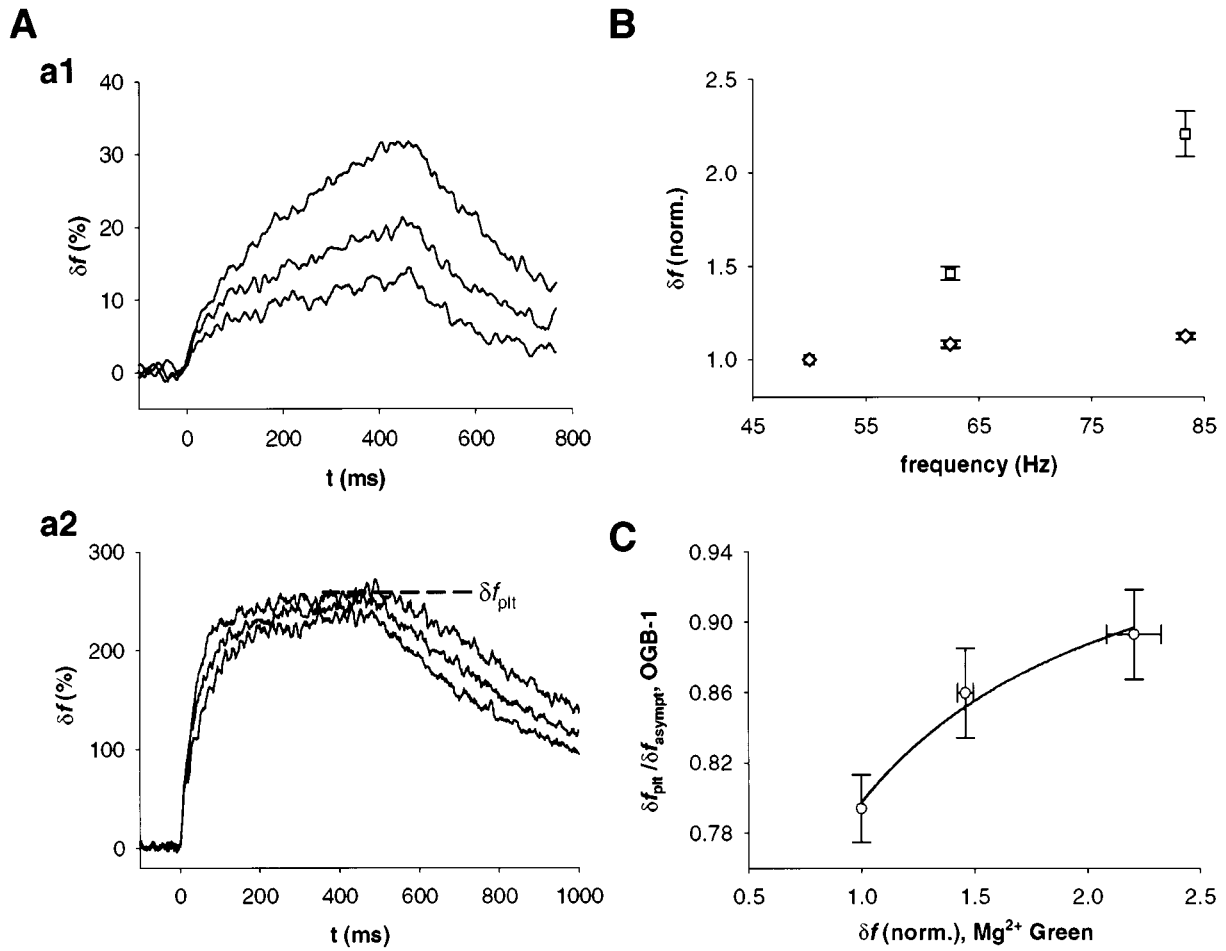

FIGURE 3 Fluorescence transients ($\delta f \equiv (f - f_0)/f_0$) in response to trains of action potentials. (*A*) Dendritic fluorescence transients evoked by AP trains at different frequencies: lowest to highest, 50 Hz, 62.5 Hz, 83.3 Hz. Dendrites were loaded with Magnesium Green (MG) (*a1*) (traces averaged over 14 trials) or with OGB-1 (*a2*) (traces averaged over five trials). *a2* indicates how OGB-1 levels δf_{plt} were determined, by averaging over saturated (plateau) portion of transients. (*B*) Fluorescence transient amplitudes as a function of frequency (from *A*). □, MG, $n = 4$; ◇, OGB-1, $n = 4$. MG levels are peak fluorescence. For OGB-1, plateau levels δf_{plt} were computed as indicated in *a2*. To compare trends, transients were normalized to the levels evoked by 50-Hz stimulation. Peak fluorescence levels as measured with MG increased approximately linearly over the range of frequencies sufficient to saturate OGB-1 saturation. (*C*) Fluorescence levels for OGB-1 plotted against levels for MG (proportional to $\Delta[Ca^{2+}]$). Levels for MG were normalized to levels evoked by 50-Hz trains, as for *B*. Fit was made to a known hyperbolic saturating relationship. OGB-1 fluorescence levels were then normalized to asymptotic value of fit, δf_{asympt}. Normalized levels therefore indicate fractional saturation for each point. Horizontal error bars indicate the SEM of normalized fluorescence ($n = 4$); vertical error bars are the quadratic sum of normalized fluorescence SEM ($n = 4$) and standard error of hyperbolic fit.

Classifying cells by postnatal age of animal (two groups: PND 14–17 and PND 24–28) did not reveal significant differences in resting $[Ca^{2+}]$. For the younger rats, $[Ca^{2+}]_0 = 36 \pm 5$ nM ($R_f = 5.7$) to 53 ± 5 nM ($R_f = 8.5$) ($n = 9$), while for the older animals $[Ca^{2+}]_0 = 40 \pm 22$ nM ($R_f = 5.7$) to 57 ± 23 nM ($R_f = 8.5$) ($n = 3$).

Endogenous buffer capacity

The peak amplitude of action potential-evoked $[Ca^{2+}]$ transients has an inverse dependence on κ_F, the added indicator buffer capacity (Eq. 8). This reflects the increasing buffering of Ca^{2+} by the added indicator. To estimate the endogenous buffer capacity κ_B, we inverted this relationship:

$$\Delta[Ca^{2+}]^{-1}(t = t_{AP}) = \frac{1 + \kappa_B}{\Delta[Ca^{2+}]_T} + \frac{\kappa_F}{\Delta[Ca^{2+}]_T}, \quad (12)$$

plotted inverse $[Ca^{2+}]$ transient amplitudes against κ_F, and fit straight lines to these data (Fig. 6). The intercept with the horizontal axis gave an estimate of κ_B (Helmchen et al., 1996). Averaged over cells ($n = 7$), values were $\kappa_B = 65 \pm 15$ ($R_f = 5.7$) or $\kappa_B = 57 \pm 13$ ($R_f = 8.5$). Classifying neurons according to age, we found the buffering capacity in those from older animals (PND 24–28) to be smaller than for younger rats (PND 14–17): for the former ($n = 3$), $\kappa_B = 48 \pm 20$ ($R_f = 5.7$) or $\kappa_B = 41 \pm 17$ ($R_f = 8.5$), while for

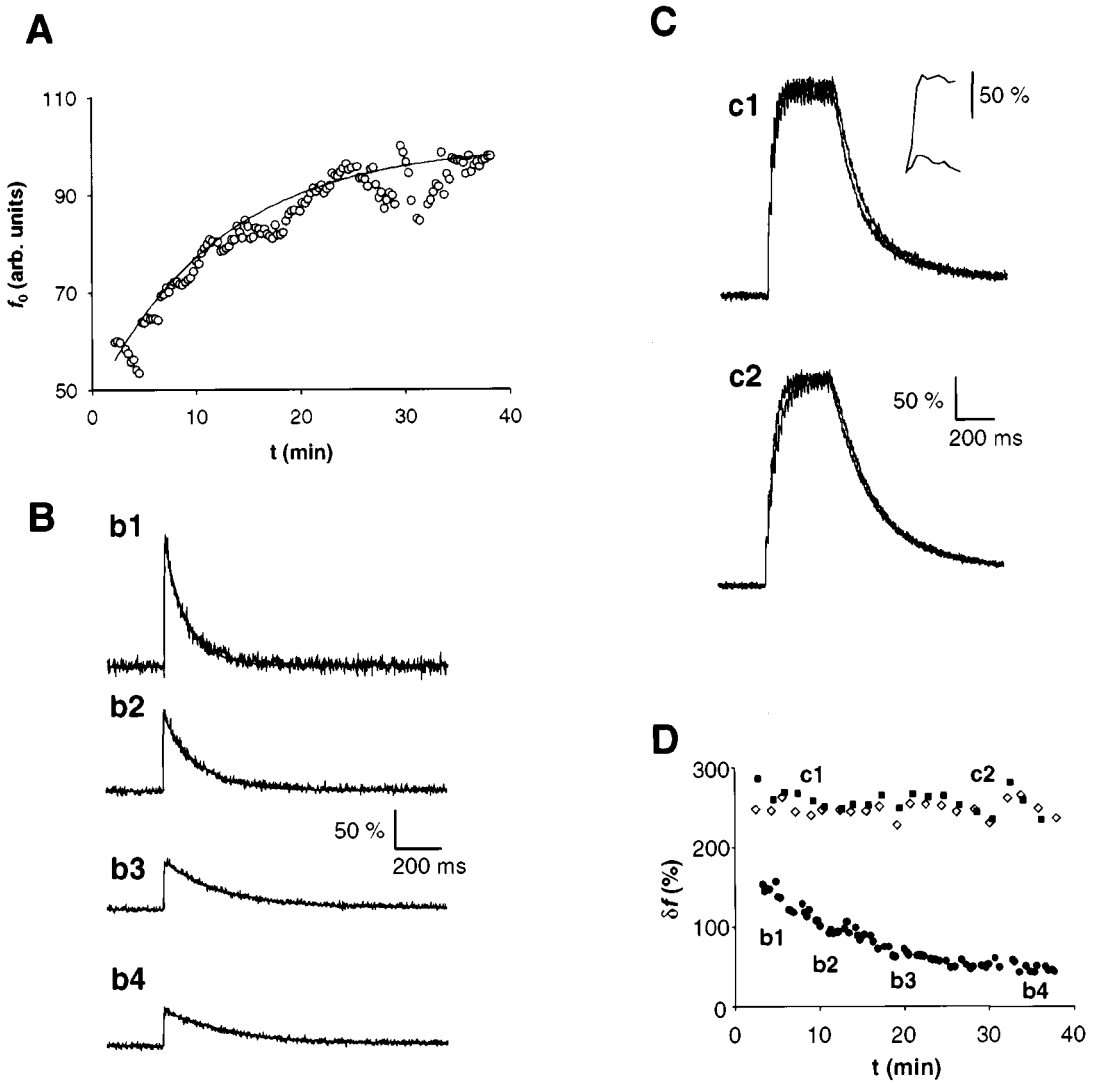

FIGURE 4 Time course of OGB-1 loading and amplitudes of fluorescence transients in a proximal apical dendrite. (*A*) The baseline fluorescence (f_0) was measured every 15 s. Occasionally the image was refocused to compensate for drift of the brain slice. The upper envelope of f_0 was fit with an exponential time course (*solid curve*). The loading time constant for this cell was 9.2 min. (*B*) Fluorescence transients (δf) evoked by single action potentials at different times after break-in (averages of three to four trials; times are indicated in *D*). Decreasing transient amplitudes and increasing durations reflect the buffering of Ca^{2+} by increasing concentrations of $[Ca^{2+}]$ indicator. (*C*) Fluorescence transients evoked by AP trains in early (*c1*) and late (*c2*) phases of loading (indicated in *D*). Transient amplitudes remained constant, reflecting constant $[Ca^{2+}]_0$ (Eq. 6). Transients due to differing stimulation frequencies (20 APs, 56 Hz; 24 APs, 67 Hz) are superimposed. The inset in *c1* shows fluorescence transients evoked (the larger) by the first AP in the train, and (the smaller) by an AP after plateau was reached. (*D*) Amplitudes of fluorescence transients as a function of loading time. Single action potential transients (●) decreased as a function of time. Transients evoked by trains (measured at plateaus; 56 Hz, ◇; 67 Hz, ■) remained constant as a function of time.

the latter ($n = 4$) $\kappa_B = 78 \pm 23$ or $\kappa_B = 68 \pm 20$ for $R_f = 5.7$ and $R_f = 8.5$, respectively. However, the difference between age groups was not significant ($p > 0.05$; Welch-Student *t*-test).

Action potential-evoked $[Ca^{2+}]$ transients

The size of the $[Ca^{2+}]$ transients induced by an action potential in the apical dendrite in the absence of an indicator can be inferred from the relationship between $\Delta[Ca^{2+}]^{-1}$ and κ_F, by extrapolating the fits to $\kappa_F = 0$ (Fig. 6). $\Delta[Ca^{2+}]$ averaged over all neurons ($n = 7$) was $\Delta[Ca^{2+}] = 235 \pm 57$ nM for $R_f = 5.7$ and $\Delta[Ca^{2+}] = 251 \pm 61$ nM for $R_f = 8.5$. Differences in buffer capacity between younger and older animals were not found to be significant: For PND 14–17, $\Delta[Ca^{2+}] = 227 \pm 65$ nM ($R_f = 5.7$), $\Delta[Ca^{2+}] = 243 \pm 70$ nM ($R_f = 8.5$) ($n = 4$), while for PND 24–28, $\Delta[Ca^{2+}] = 245 \pm 138$ nM ($R_f = 5.7$), $\Delta[Ca^{2+}] = 262 \pm 148$ nM ($R_f = 8.5$) ($n = 3$). A summary of the data presented in this section is contained in Table 2.

TABLE 2 [Ca^{2+}] regulation in the apical dendrites of CA1 pyramidal neurons

Parameter	PND 14–17	PND 24–28	Overall
δf_{max} (%)			
Mean	240	243	241
Range	190–317	152–296	152–317
N	9	3	12
$\Delta[Ca^{2+}]$ (nM)			
Mean	237	255	245
Range	162–313	107–410	178–312
N	4	3	7
κ_B			
Mean	73	44	61
Range	48–101	24–68	44–80
N	4	3	7
$[Ca^{2+}]_0$ (nM)			
Mean	46	50	47
Range	31–58	19–81	32–59
N	9	3	12

Column headings indicate age of rats in postnatal days (PND). Values were computed as follows: δf_{max} is given as a range from the minimum to the maximum value recorded across the neurons used for data analysis (average ± SEM across neurons was 241 ± 15%). Means were computed by assuming R_f halfway between its cuvette and in situ values. Ranges are defined by mean − SEM for R_f giving the smallest value, and mean + SEM for R_f giving the largest value.

DISCUSSION

Because of signal-to-noise ratio considerations, high-affinity $[Ca^{2+}]$ indicators with large dynamic ranges are especially well suited for $[Ca^{2+}]$ estimation in small neuronal compartments (Muller and Connor, 1991; Murphy et al., 1994; Yuste and Denk, 1995; Denk et al., 1995; Koester and Sakmann, 1998; Mainen et al., 1999b). Based on the fluorescence signal evoked by a stimulus, it is often of interest to compute an experimental measure proportional to the corresponding evoked $\Delta[Ca^{2+}]$. The fractional fluorescence change $\delta f \equiv (f - f_0)/f_0$ has this property, but only in the linear regime of the indicator ($[Ca^{2+}] \ll K_D$). High-affinity indicators show sublinear δf even when challenged with modest $[Ca^{2+}]$ transients (cf. Fig. 1). Additional problems with measurement of δf are encountered during prolonged experiments: δf might decrease simply because f_0 increases, because of small changes in resting $[Ca^{2+}]$, or because of photodamage (Koester et al., 1999) or bleaching. Furthermore, for a given Ca^{2+} current and resting $[Ca^{2+}]$, δf decreases with increasing indicator concentration, because of Ca^{2+} buffering.

We have described a method (Eqs. 4, 5, and 7) to correct for the nonlinear response of a Ca^{2+} indicator to obtain accurate estimates of $\Delta[Ca^{2+}]$ and absolute $[Ca^{2+}]$. This method relies on information gained by measuring the maximum relative fluorescence level in the structure of interest, δf_{max}, during an experiment. The calculation of $[Ca^{2+}]$ requires estimates of two additional parameters: the dissociation constant, K_D, and the dynamic range, R_f, of the

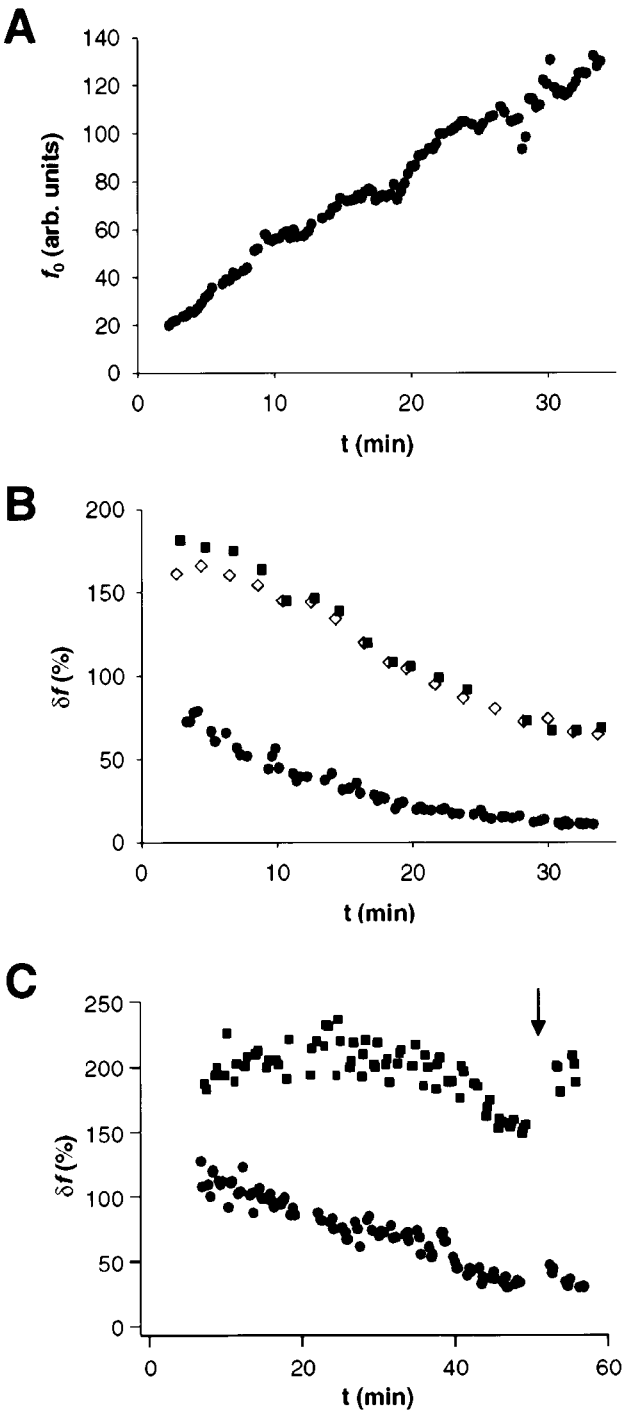

FIGURE 5 Changes in fluorescence as markers of resting $[Ca^{2+}]_0$ and cell health. (*A*) Time course of resting fluorescence. After ~40 min of loading no steady state had been reached. (*B*) Amplitudes of fluorescence transients (same cell). Single-AP transients (●) decreased with loading, as did transients evoked by trains at two different frequencies (56 Hz, ◇; 67 Hz, ■), suggesting an increase in resting $[Ca^{2+}]$ (Eq. 6). (*C*) As in *B*, for a different cell. After δf_{max} decreased, imaging in an adjacent dendritic region (~5 μm from the first point; indicated by *arrow*) recovered the signal. This suggested that the local drop in δf_{max} was due to local photodamage while $[Ca^{2+}]_0$ remained constant.

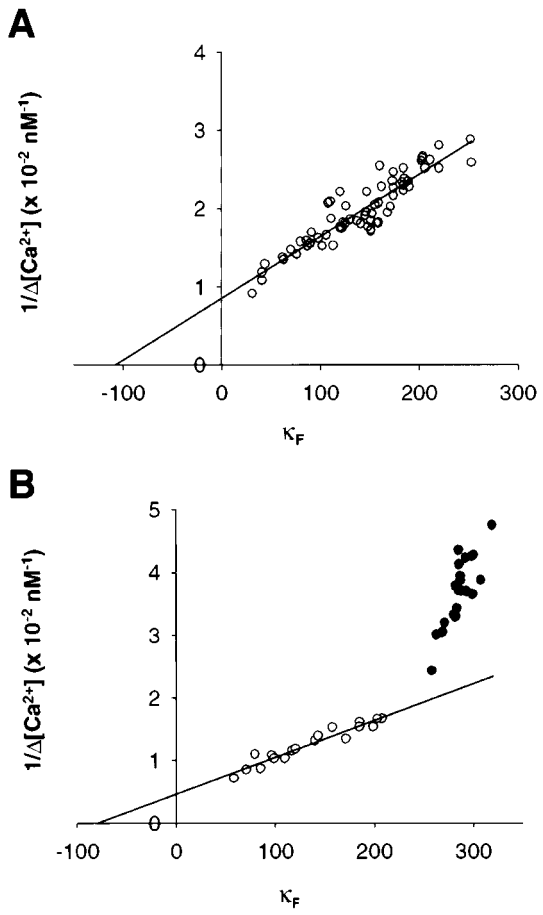

FIGURE 6 Estimating the endogenous buffer capacity. (*A*) Inverse single-AP peak $[Ca^{2+}]$ transient increase, $\Delta[Ca^{2+}]^{-1}$, versus added buffer capacity, κ_F, for a cell from a young animal. Endogenous capacity was computed from the fit's intersection with the *x* axis and was between $\kappa_B = 106 \pm 10$ ($r = 0.92$) (computed with $R_f = 5.7$) and $\kappa_B = 93 \pm 9$ ($r = 0.92$) ($R_f = 8.5$). (*B*) As in *A*, for a cell from an older animal. Endogenous capacity was between $\kappa_B = 78 \pm 2$ ($r = 0.96$) ($R_f = 5.7$) and $\kappa_B = 68 \pm 2$ ($r = 0.96$) ($R_f = 8.5$) based on fit to the early part of the experiment (○). Note the pronounced convexity in the curve and the increased slope of later points (●), suggesting a decrease in the amplitudes of the Ca^{2+} current.

indicator. Because the calibration parameters are properties of an indicator and would not be expected to vary across cells of a given type, they do not need to be evaluated during every experiment. Nevertheless, because these parameters may be sensitive to the nature of the intracellular environment, it is important to consider sources of error in calibrations based on estimates of R_f and K_D (Appendix B).

Parameter calibration and robustness of the method

We estimated a lower bound for the dynamic range of Oregon Green BAPTA-1 in CA1 pyramidal neurons in hippocampal slices, comparing f_{max} with minimum fluorescence levels obtained by washing in an extracellular solution containing zero $[Ca^{2+}]$ and high EGTA. Our results gave a bound equal to ~50–70% of the value of R_f measured in vitro, which is consistent with previous experiments conducted with other Ca^{2+} indicators (O'Malley et al., 1999; Harkins et al., 1993). Because our procedure did not allow us to clamp intracellular $[Ca^{2+}]$ to zero, intracellular values of R_f may be closer to the in vitro estimate of 8.5; in any case R_f is constrained between 5.7 and 8.5.

Importantly, the estimates of $\Delta[Ca^{2+}]$ obtained with our method were quite insensitive to the exact value used for R_f. For example, our estimates of the amplitude of single action potential $[Ca^{2+}]$ transients at zero added buffer (cf. Helmchen et al., 1996) varied by less than 10% over the range $R_f \approx 5.7–8.5$ (for an interpretation see Fig. 1 *B*). Our estimates of absolute $[Ca^{2+}]$ were less robust, varying by up to ~40% in the range $R_f \approx 5.7–8.5$ (Eq. 11). These variations are predicted by error propagation analysis (Appendix B).

We estimated the dissociation constant of the indicator, K_D, in intracellular solution but not in intact cells. This quantity may be quite different in the intracellular environment: a correction of >30% is expected (Minta et al., 1989). Because K_D appears only as a scale factor in all relevant equations (Eqs. 4, 5, and 7), this correction would apply directly to all $[Ca^{2+}]$ estimates and our derivations of κ_B. A similar scaling factor applies to measurements with ratiometric indicators.

With the method presented, the fluorescence at saturating $[Ca^{2+}]$, f_{max}, is measured periodically during each experiment at the same position where $[Ca^{2+}]$ measurements are being obtained. In most neurons, this can be achieved by eliciting trains of action potentials to flood the neuron with Ca^{2+} entering through voltage-gated Ca^{2+} channels (Figs. 3 and 4).

Because of the weak dependence of fluorescence on $[Ca^{2+}]$ at large concentrations (where $[Ca^{2+}] \gg K_D$) (Fig. 1), even relatively high-frequency action potential trains (67 Hz) produced only ~70–90% saturation in our experiments in CA1 dendrites. This relatively large variation in saturation level may partly reflect differences in action potential-evoked $[Ca^{2+}]$ transients, depending on distance from the soma (range 30–70 μm; Regehr et al., 1989; Magee and Johnston, 1997; Svoboda et al., 1999). Thus estimates of $[Ca^{2+}]$ based simply on the plateau fluorescence reached during a high-frequency train may result in relatively large measurement errors (up to ~30% for the measurements presented here; see also Appendix B). These errors grow as f approaches f_{max}. However, the estimate can be improved considerably if fluorescence transients are measured at more than one frequency, allowing extrapolation to true δf_{max}. This necessitates making an assumption about the true nature of AP-evoked $\Delta[Ca^{2+}]$. For instance, our technique relies on the proportionality of $[Ca^{2+}]$ increases to AP frequency (Eq. 11), which was verified by parallel measurements with the low-affinity indicator MG.

However, saturation can be verified even in cases where this assumption does not hold. Assume, for instance, that $[Ca^{2+}]$ accumulations evoked by each action potential in a train have equal sizes at different frequencies. (Although this assumption is similar to the one above, it does not imply a constant Ca^{2+} removal rate.) The assumption would be invalid if Ca^{2+} influx suffered from greater rundown at higher frequencies, but can be tested by comparing fluorescence transients elicited by individual action potentials at the beginning and at the end of an AP train. This alternative assumption also allows extrapolation to true δf_{max}. For instance, using it we recomputed the level of saturation for the AP train-evoked transients shown in Fig. 4, which are 89% saturated, assuming proportionality to frequency as described above. This compares to a value of 93%, using the assumption just introduced, in approximate agreement. Therefore our method does not require proportionality between $[Ca^{2+}]$ accumulations and AP frequency.

Measurements of intracellular Ca^{2+} levels and regulation

In addition to permitting accurate calibration of $[Ca^{2+}]$ and $\Delta[Ca^{2+}]$, measurements of saturating fluorescence transients during an experiment have other benefits. For example, for healthy neurons with constant $[Ca^{2+}]_0$, the ratio of saturating fluorescence transient over resting fluorescence, δf_{max}, should remain constant, independent of changes in indicator concentration. We found this behavior in most neurons over periods of up to 1 h (see, e.g., Fig. 4). However, other neurons showed a decreasing δf_{max}, suggesting an increasing resting $[Ca^{2+}]$ (Fig. 5). This could be distinguished from subcellular compartmentalization of indicator or photoinduced changes in fluorescence (Konig et al., 1999; Koester et al., 1999) by verifying whether transient size varied as the imaging region was moved to an adjacent position along the dendrite (Fig. 5 *C*).

Measurements of $[Ca^{2+}]$ regulation in hippocampal pyramidal cells reported in this paper are mostly similar to values previously reported with ratiometric indicators. The range of $[Ca^{2+}]_0$ was 32–59 nM, at the low end of the range reported in cultured neurons (Nakajima et al., 1993), and distributed over a narrower range, perhaps reflecting our method's accuracy. Single action potential $[Ca^{2+}]$ transients were, on average, around 250 nM, somewhat higher than previous pyramidal cell estimates (Helmchen et al., 1996). Dendritic intracellular buffer capacity (κ_B) had a mean of ~60, slightly smaller than in previous measurements (Helmchen et al., 1996). In some neurons, plots of inverse $\Delta[Ca^{2+}]$ versus added buffer capacity showed a distinct late convex upswing (Fig. 6 *B*), without changes in δf_{max}, suggesting a late decrease in total calcium current. There were no statistically significant differences in resting $[Ca^{2+}]$, average $[Ca^{2+}]$ transient size per action potential, or buffering capacity between animals of different age groups (PND 14–17 and PND 24–28).

APPENDIX A: ESTIMATING SATURATION BY COMPARING FLUORESCENCE PLATEAUS EVOKED AT DIFFERENT FREQUENCIES (DERIVATION OF EQ. 11)

At the steady-state $[Ca^{2+}]$ plateau evoked by an AP train at sufficiently high frequency (Regehr et al., 1994; Helmchen et al., 1996), the change in fluorescence from rest increases with the change in calcium bound to dye:

$$\Delta f_{plt} \propto \left(\frac{[Ca^{2+}]_{plt}}{K_D + [Ca^{2+}]_{plt}} - \frac{[Ca^{2+}]_0}{K_D + [Ca^{2+}]_0} \right) = \frac{K_D \Delta[Ca^{2+}]_{plt}}{(K_D + \Delta[Ca^{2+}]_{plt} + [Ca^{2+}]_0)(K_D + [Ca^{2+}]_0)}. \quad (A1)$$

Consequently, the ratio Q of fluorescence plateaus generated at two different frequencies ν_2 and ν_1 ($\nu_2 > \nu_1$) is

$$Q \equiv \frac{(\Delta f_{plt}/f_0)_2}{(\Delta f_{plt}/f_0)_1} = \frac{(\Delta[Ca^{2+}]_{plt})_2}{(\Delta[Ca^{2+}]_{plt})_1} \left(\frac{K_D + (\Delta[Ca^{2+}]_{plt})_1 + [Ca^{2+}]_0}{K_D + (\Delta[Ca^{2+}]_{plt})_2 + [Ca^{2+}]_0} \right). \quad (A2)$$

With the simplifying notation $\Delta_1 \equiv (\Delta[Ca^{2+}]_{plt})_1$, the second factor on the right-hand side of this expression is

$$\frac{K_D + \Delta_1 + [Ca^{2+}]_0}{K_D + \Delta_2 + [Ca^{2+}]_0} = 1 + \frac{\Delta_2}{K_D + \Delta_2 + [Ca^{2+}]_0} \left(\frac{\Delta_1}{\Delta_2} - 1 \right). \quad (A3)$$

Because resting $[Ca^{2+}]$ is within the linear limit of the dye, i.e., it is much smaller than K_D and Δ_2, this expression can be written approximately as

$$\begin{aligned} 1 + \frac{\Delta_2}{K_D + \Delta_2 + [Ca^{2+}]_0} \left(\frac{\Delta_1}{\Delta_2} - 1 \right) &\cong 1 + \frac{\Delta_2 + [Ca^{2+}]_0}{K_D + \Delta_2 + [Ca^{2+}]_0} \left(\frac{\Delta_1}{\Delta_2} - 1 \right) \\ &= 1 + \frac{([Ca^{2+}]_{plt})_2}{K_D + ([Ca^{2+}]_{plt})_2} \left(\frac{\Delta_1}{\Delta_2} - 1 \right) \\ &= 1 + \frac{([FCa]_{plt})_2}{[F]_T} \left(\frac{\Delta_1}{\Delta_2} - 1 \right). \end{aligned} \quad (A4)$$

The ratio between concentrations in the last expression is simply $x/100$, the degree of saturation of the fluorophore at the $[Ca^{2+}]$ plateau induced by stimulation at frequency ν_2. If transients are proportional to frequency as assumed, then $\Delta_1/\Delta_2 = \nu_1/\nu_2$ and

$$Q = \frac{\nu_2}{\nu_1} \left[1 + x/100 \left(\frac{\nu_1}{\nu_2} - 1 \right) \right]. \quad (A5)$$

APPENDIX B: PROPAGATION OF PARAMETER CALIBRATION ERRORS

Calibration errors can arise from erroneous estimation of the parameters R_f, δf_{max}, and K_D. Errors in K_D will simply have a multiplicative effect.

Errors in estimating the dynamic range will give a value $R'_f = \rho R_f$, where R_f is the correct value and the multiplicative factor ρ is close to 1 (for instance, if R_f is really around 6 but is estimated to be its cuvette value $R_f \approx 8.5$, $\rho \approx 1.4$). This will result in an estimate of $[Ca^{2+}]$ that relates to the true value as follows:

$$\frac{[Ca^{2+}]'}{K_D} = \frac{[Ca^{2+}]}{K_D} + \frac{\rho - 1}{R'_f(1 - f/f_{max})}. \quad \text{(B1)}$$

The relative error in measured $[Ca^{2+}]$ as compared to the correct value is then

$$(\theta[Ca^{2+}])_R \equiv \frac{[Ca^{2+}]' - [Ca^{2+}]}{[Ca^{2+}]} = \frac{\rho - 1}{R'_f f/f_{max} - \rho}. \quad \text{(B2)}$$

This quantity is of practical interest because it provides a higher bound on the relative error in $[Ca^{2+}]$ caused by erroneous estimation of the dynamic range. For any experiment one can define a lower bound to R_f given by the ratio of saturated and resting fluorescences, f_{max}/f_0. Therefore there is a higher bound for ρ and there follows a higher bound for the possible relative error. For $\Delta[Ca^{2+}]$ the relative error induced by an incorrect calibration of R_f is

$$(\theta\Delta[Ca^{2+}])_R = \frac{\rho - 1}{R'_f - \rho}. \quad \text{(B3)}$$

This expression is not directly dependent on f or δf_{max} and is more robust than the absolute concentration against errors in determination of R_f. For example, if $R'_f = 8.5$ and $\rho \leq 1.5$ (values quoted in the main text), then the relative error is $(\theta\Delta[Ca^{2+}])_R \leq 7\%$.

Underestimation of the saturating fluorescence f_{max} affects measurements of resting calcium levels less than does overestimation of R_f. However, errors in f_{max} greatly distort measurements at the upper end of the dye's dynamic range. With an estimated value $f'_{max} = \varphi f_{max}$ ($\varphi < 1$), calcium concentration will be overestimated as

$$\frac{[Ca^{2+}]'}{K_D} = \frac{[Ca^{2+}]}{K_D} + \frac{(1 - \varphi)(1 - R_f^{-1})f/f'_{max}}{(1 - f/f'_{max})(1 - \varphi f/f'_{max})}, \quad \text{(B4)}$$

which is a relative error of

$$(\theta[Ca^{2+}])_f = \frac{(1 - \varphi)(1 - R_f^{-1})f/f'_{max}}{(1 - f/f'_{max})(\varphi f/f'_{max} - R_f^{-1})} \quad \text{(B5)}$$

with respect to the true $[Ca^{2+}]$. For $\Delta[Ca^{2+}]$,

$$(\theta\Delta[Ca^{2+}])_f = \frac{(1 - \varphi)(1/\varphi - f/f'_{max}f_0/f'_{max})}{(1 - f/f'_{max})(1 - f_0/f'_{max})}. \quad \text{(B6)}$$

Underestimates of δf_{max}, $\delta f'_{max} = \gamma\delta f_{max}$ ($\gamma < 1$), result in overestimates of $[Ca^{2+}]_0$ when this quantity is computed according to Eq. 7:

$$\frac{[Ca^{2+}]'_0}{K_D} = \frac{[Ca^{2+}]_0}{K_D} + \frac{(1 - \gamma)(1 - R_f^{-1})}{\delta f'_{max}}. \quad \text{(B7)}$$

The corresponding relative error is

$$(\theta[Ca^{2+}]_0)_{\delta f} = (1 - \gamma)\frac{1 - R_f^{-1}}{\gamma(1 - R_f^{-1}) - R_f^{-1}\,\delta f'_{max}}. \quad \text{(B8)}$$

For a typical fractional saturation value of 87% (see main text), and with $R_f = 5.7$ and $\delta f'_{max} = 2.2$, this is $(\theta[Ca^{2+}]_0)_{\delta f} \leq 32\%$. Overestimating R_f ($R'_f = \rho R_f$, $\rho > 1$) leads, based on this equation, to an overestimate of $[Ca^{2+}]_0$ equal to

$$\frac{[Ca^{2+}]'_0}{K_D} = \frac{[Ca^{2+}]_0}{K_D} + \frac{\rho - 1}{R'_f}(1 + 1/\delta f_{max}), \quad \text{(B9)}$$

or in relative terms,

$$(\theta[Ca^{2+}]_0)_R = (\rho - 1)\frac{1 + \delta f_{max}}{R'_f - \rho(1 + \delta f_{max})}. \quad \text{(B10)}$$

For the values quoted in the main text $R'_f = 8.5$ and $\rho \leq 1.5$, and for a typical value of $\delta f_{max} = 2.2$, this is $(\theta[Ca^{2+}]_0)_R \leq 42\%$.

We thank Barry J. Burbach for excellent technical assistance, Esther Nimchinsky for providing slice cultures, and D. M. O'Malley for a critical reading of the manuscript.

Supported by the Swartz (MM), Burroughs Wellcome (ZFM), Helen Hay Whitney (BLS), Whitaker, Klingenstein, and Mathers Foundations and the National Institutes of Health (KS).

REFERENCES

Bers, D. M., C. W. Patton, and R. Nuccitelli. 1994. A practical guide to the preparation of Ca^{2+} buffers. *Methods Cell Biol.* 40:3–29.

Busa, W. B. 1992. Spectral characterization of the effect of viscosity on Fura-2 fluorescence: excitation wavelength optimization abolishes the viscosity artifact. *Cell Calcium.* 13:313–319.

Denk, W., J. H. Strickler, and W. W. Webb. 1990. Two-photon laser scanning microscopy. *Science.* 248:73–76.

Denk, W., M. Sugimori, and R. Llinas. 1995. Two types of calcium response limited to single spines in cerebellar Purkinje cells. *Proc. Natl. Acad. Sci. USA.* 92:8279–8282.

Denk, W., and K. Svoboda. 1997. Photon upmanship: why multiphoton imaging is more than a gimmick. *Neuron.* 18:351–357.

Feller, M. B., K. R. Delaney, and D. W. Tank. 1996. Presynaptic calcium dynamics at the frog retinotectal synapse. *J. Neurophysiol* 76:381–400.

Grynkiewicz, G., M. Poenie, and R. Y. Tsien. 1985. A new generation of Ca^{2+} indicators with greatly improved fluorescence properties. *J. Biol. Chem.* 260:3440–3450.

Harkins, A. B., N. Kurebayashi, and S. M. Baylor. 1993. Resting myoplasmic free calcium in frog skeletal muscle fibers estimated with fluo-3. *Biophys. J.* 65:865–881.

Haugland, R. P. 1996. Handbook of Biological Fluorescent Probes and Research Chemicals. Molecular Probes, Eugene, OR.

Helmchen, F., K. Imoto, and B. Sakmann. 1996. Ca^{2+} buffering and action potential-evoked Ca^{2+} signaling in dendrites of pyramidal neurons. *Biophys. J.* 70:1069–1081.

Jaffe, D. B., D. Johnston, N. Lasser-Ross, J. E. Lisman, H. Miyakawa, and W. N. Ross. 1992. The spread of Na^+ spikes determines the pattern of dendritic Ca^{2+} entry into hippocampal neurons. *Nature.* 357:244–246.

Kao, J. P., A. T. Harootunian, and R. Y. Tsien. 1989. Photochemically generated cytosolic calcium pulses and their detection by fluo-3. *J. Biol. Chem.* 264:8179–8184.

Kennedy, H. J., and R. C. Thomas. 1996. Effects of injecting calcium-buffer solution on $[Ca^{2+}]_i$ in voltage-clamped snail neurons. *Biophys. J.* 70:2120–2130.

Koester, H. J., D. Baur, R. Uhl, and S. W. Hell. 1999. Ca^{2+} fluorescence imaging with pico- and femtosecond two-photon excitation: signal and photodamage. *Biophys. J.* 77:2226–2236.

Koester, H. J., and B. Sakmann. 1998. Calcium dynamics in single spines during coincident pre- and postsynaptic activity depend on relative timing of back propagating action potentials and subthreshold excitatory postsynaptic potentials. *Proc. Natl. Acad. Sci. USA.* 95:9596–9601.

Konig, K., T. W. Becker, P. Fisher, I. Riemann, and K. J. Halbhuber. 1999. Pulse-length dependence of cellular response to intense near-infrared laser pulses in multiphoton microscopes. *Optics Lett.* 24:113–115.

Kurebayashi, N., A. B. Harkins, and S. M. Baylor. 1993. Use of fura red as an intracellular calcium indicator in frog skeletal muscle fibers. *Biophys. J.* 64:1934–1960.

Lau, P. M., R. S. Zucker, and D. Bentley. 1999. Induction of filopodia by direct local elevation of intracellular calcium ion concentration. *J. Cell Biol.* 145:1265–1275.

Lev-Ram, V., H. Miyakawa, N. Lasser-Ross, and W. N. Ross. 1992. Calcium transients in cerebellar Purkinje neurons evoked by intracellular stimulation. *J. Neurophysiol.* 68:1167–1177.

Magee, J. C., and D. Johnston. 1997. A synaptically controlled, associative signal for Hebbian synaptic plasticity in hippocampal neurons. *Science.* 275:209–213.

Mainen, Z. F., M. Maletic-Savatic, S. H. Shi, Y. Hayashi, R. Malinow, and K. Svoboda. 1999a. Two-photon imaging in living brain slices. *Methods: Comp. Methods Enzymol.* 18:231–239.

Mainen, Z. F., R. Malinow, and K. Svoboda. 1999b. Synaptic calcium transients in single spines indicate that NMDA receptors are not saturated. *Nature.* 399:151–155.

Markram, H., P. J. Helm, and B. Sakmann. 1995. Dendritic calcium transients evoked by single back-propagating action potentials in rat neocortical pyramidal neurons. *J. Physiol. (Lond.).* 485:1–20.

Minta, A., J. P. Kao, and R. Y. Tsien. 1989. Fluorescent indicators for cytosolic calcium based on rhodamine and fluorescein chromophores. *J. Biol. Chem.* 264:8171–8178.

Muller, W., and J. A. Connor. 1991. Dendritic spines as individual neuronal compartments for synaptic Ca^{2+} responses. *Nature.* 354:73–76.

Murphy, T. H., J. M. Baraban, W. G. Wier, and L. A. Blatter. 1994. Visualization of quantal synaptic transmission by dendritic calcium imaging. *Science.* 263:529–532.

Nakajima, K., K. Harada, Y. Ebina, T. Yoshimura, H. Ito, T. Ban, and R. Shingai. 1993. Relationship between resting cytosolic Ca^{2+} and responses induced by *N*-methyl D-aspartate in hippocampal neurons. *Brain Res.* 603:321–323.

Neher, E., and G. J. Augustine. 1992. Calcium gradients and buffers in bovine chromaffin cells. *J. Physiol. (Lond.).* 450:273–301.

O'Malley, D. M. 1994. Calcium permeability of the neuronal nuclear envelope: evaluation using confocal volumes and intracellular perfusion. *J. Neurosci.* 14:5741–5758.

O'Malley, D. M., B. Burbach, and P. Adams. 1999. Fluorescent calcium indicators: subcellular behavior and use in confocal imaging. *In* Protocols in Confocal Microscopy. S. Paddock, editor. Humana Press, New York.

Regehr, W. G., and P. P. Atluri. 1995. Calcium transients in cerebellar granule cell presynaptic terminals. *Biophys. J.* 68:2156–2170.

Regehr, W. G., J. A. Connor, and D. W. Tank. 1989. Optical imaging of calcium accumulation in hippocampal pyramidal cells during synaptic activation. *Nature.* 341:533–536.

Regehr, W. G., K. R. Delaney, and D. W. Tank. 1994. The role of presynaptic calcium in short-term enhancement at the mossy fiber synapse. *J. Neurosci.* 14:523–537.

Sabatini, B. L., and W. G. Regehr. 1998. Optical measurement of presynaptic calcium currents. *Biophys. J.* 74:1549–1563.

Schiller, J., F. Helmchen, and B. Sakmann. 1995. Spatial profile of dendritic calcium transients evoked by action potentials in rat neocortical pyramidal neurons. *J. Physiol. (Lond.).* 487:583–600.

Schiller, J., Y. Schiller, and D. E. Clapham. 1998. NMDA receptors amplify calcium influx into dendritic spines during associative pre- and postsynaptic activation. *Nature Neurosci.* 1:114–118.

Schiller, J., Y. Schiller, G. Stuart, and B. Sakmann. 1997. Calcium action-potentials restricted to distal apical dendrites of rat neocortical pyramidal neurons. *J. Physiol. (Lond.).* 505:605–616.

Svoboda, K., W. Denk, D. Kleinfeld, and D. W. Tank. 1997. In vivo dendritic calcium dynamics in neocortical pyramidal neurons. *Nature.* 385:161–165.

Svoboda, K., F. Helmchen, W. Denk, and D. W. Tank. 1999. The spread of dendritic excitation in layer 2/3 pyramidal neurons in rat barrel cortex in vivo. *Nature Neurosci.* 2:65–73.

Tsien, R. Y. 1989. Fluorescent probes for cell signalling. *Annu. Rev. Neurosci.* 12:227–253.

Tsien, R., and T. Pozzan. 1989. Measurement of cytosolic free Ca^{2+} with quin2. *Methods Enzymol.* 172:230–262.

Tsien, R. Y., and A. Waggoner. 1995. Fluorophores for confocal microscopy. *In* Handbook of Biological Confocal Microscopy. J. B. Pawley, editor. Plenum Press, New York. 267–279.

Yuste, R., and W. Denk. 1995. Dendritic spines as basic functional units of neuronal integration. *Nature.* 375:682–684.